JOURNAL OF AIRCRAFT
Vol. 47, No. 4, July–August 2010

Engineering Notes

Bubble Burst Control Using Smart Structure Sensor Actuators for Stall Suppression

Chi Wai Wong* and Kenichi Rinoie†
University of Tokyo, Tokyo 113-8656, Japan

DOI: 10.2514/1.46905

I. Introduction

AFTER the laminar boundary layer separates from the airfoil surface, the flow can reattach to the surface as a turbulent shear layer. The region between the laminar separation and the reattachment is called a laminar separation bubble [1]. Depending on the chordwise extent of the laminar separation bubble, it can be classified as a short bubble or a long bubble. Once the short bubble fails to reattach on the airfoil surface, which is commonly known as short-bubble burst, this causes the airfoil to stall abruptly. Methods do exist to predict the short bubble [2]. Active flow control methods such as oscillatory blowing [3], plasma [4], and piezoelectric [5] actuators are useful methods for flow separation delay. Previous studies conducted by Rinoie et al. [6], the control of the short-bubble burst was proposed. Their work considered the control of the separated shear layer development artificially and their experimental results confirmed that the use of a thin plate placed on a NACA 0012 airfoil was effective for suppression of laminar separation-bubble burst formed on the leading edge of the airfoil and increased both the stall angle and the maximum lift coefficient (approximately 10% increment, as compared with the clean airfoil) at a chord Reynolds number of 1.3×10^5. The particle image velocimetry data also revealed that the vortical structures originated from Kelvin–Helmholtz instability inside the separated shear layer are enhanced by those formed at the trailing edge of the plate, and this forces the separated shear layer to reattach downstream of the plate. More recently, the effectiveness of both the thin and rectangular plates was examined [7] on a NACA 631-012 airfoil at a chord Reynolds number of 1.3×10^5. The maximum lift coefficient of the airfoil with plate attachment (obtained from the total force measurements) was approximately 17% higher than the value of the clean airfoil (i.e., airfoil without plate attachment). The stall angle of the airfoil with the plate attachment was postponed. However, the use of both the thin and rectangular plates at any angle of attack less than 9° was detrimental to the flowfield on the suction surface of the airfoil. The lift-to-drag ratio of the airfoil with plate attachment was found to be significantly less than the values of the clean airfoil. Their data were also insufficient for an exact determination of the optimum configuration, including the height, location, and width of the plate.

Presented as Paper 2009-4277 at the 39th AIAA Fluid Dynamics Conference, San Antonio, TX, 22–25 June 2009; received 28 August 2009; revision received 8 April 2010; accepted for publication 9 April 2010.

*JSPS Postdoctoral Fellow, Department of Aeronautics and Astronautics, School of Engineering, 7-3-1 Hongo, Bunkyo-ku. Senior Member AIAA.

†Professor, Department of Aeronautics and Astronautics, School of Engineering, 7-3-1 Hongo, Bunkyo-ku. Senior Member AIAA.

According to the literature [4,8,9], there are many methods available that identify the incipient flow separation on the suction side of airfoils. The methods often correlate the pressure fluctuations, flow directions, and shear stress with physical phenomena such as laminar separation. Though the methods developed in [4,8,9] were used in conjunction with other flow control mechanisms, they provide useful information on the development of the smart structure sensor actuator system in the current study. The ultimate goal of the present work is to develop a smart structure sensor actuator system (in short, autonomous actuation system) that can be used to enhance the application of the burst control plate attached to the leading edge of the airfoil and to serve as a stall-avoidance system. The pressure amplitude near the leading edge of the airfoil provides simple and valuable information and is used for the feedback control rule for adjusting the plate penetration into the flow during the airfoil pitch-up.

II. Experimental Details

Measurements were conducted in a subsonic suction type wind tunnel with freestream turbulent intensity of 0.16% at a freestream velocity of 10 m/s. A NACA 631-012 airfoil with span of 200 mm and chord length of 200 mm was employed. The Reynolds number based on the chord length is 1.3×10^5. Three pressure taps (note that the differential pressure sensors are situated outside the test section) are located upstream of the burst control plate, and their chordwise locations from the leading edge of the airfoil are 2, 3, and 4 mm (indicated as P3, P2, and P1, respectively, in Fig. 1) and their nondimensionalized values (i.e., divided by the airfoil chord length) are 0.01, 0.015 and 0.02, respectively. The pressure range of the differential pressure sensor manufactured by Honeywell is ± 63.5 mm H_2O and the repeatability for the pressure measurement is approximately $\pm 0.25\%$. On the other hand, three photo interrupters that are used as displacement sensors (indicated as D1, D2, and D3 in Fig. 1) were installed underneath the thin plate (hereafter referred to as the burst control plate) and they are to measure the trailing-edge height of the burst control plate. The displacement sensor has a measure range from 0 to 5 mm and the accuracy for the plate height measurement is approximately $\pm 0.1\%$. The height of the burst control plate is controlled by the angular movement of two identical micro servos that are typically used for radio-controlled planes. The micro servos implemented in the airfoil section are to be used as small-scale actuators and they are located on either end of the airfoil section (indicated as A1 and A2 in Fig. 1). Note that the torque provided by each micro servo is 0.177 Nm. The maximum angular movement of the micro servo is about 60°, and this limits the maximum height of the burst control plate to approximately 1.2 mm. Note that the airfoil section displayed in Fig. 1 is an incomplete model. Since the sensors on the airfoil are coupled with different small tubes and electric wires, every possible effort was made to minimize the interference with the force measurements. Also, the hole on the test section where the tubes and cables pass through was covered with a Perspex box to avoid pressure loss.

The thin plate with a thickness of 0.3 mm (which is located on the suction side of the airfoil model), also known as the burst control plate, used in the present study is geometrically similar to the one studied in [6,7], but the dimensions of the plate are different. The chordwise length of the burst control plate is 5 mm and the value after being nondimensionalized with the airfoil chord length is 0.025. The location of the plate is defined by the distance between the leading edge of the airfoil and the trailing edge of the plate, and it is indicated as x_p. In the current investigation, x_p is 12 mm and the value after being nondimensionalized with the airfoil chord length is 0.06. The height of the trailing edge of the burst control plate is defined as h.

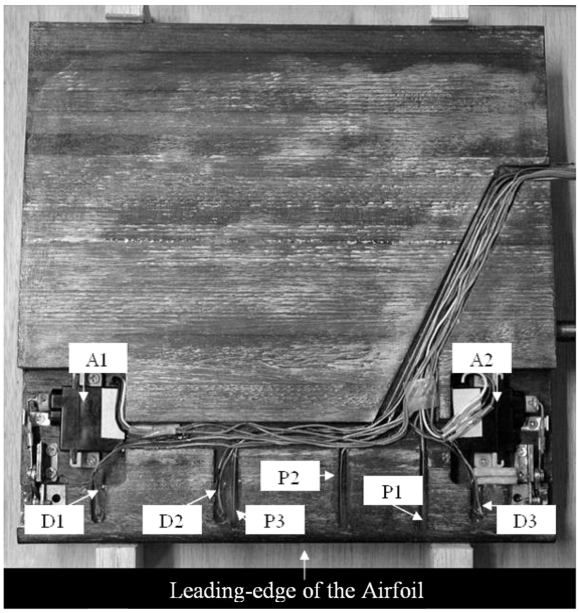

Fig. 1 Overall configuration of the devices installed in the lower side of the airfoil section.

When the disc of the actuator rotates, it pushes the connection rod (i.e., the one that connects to the small-scale actuator) downward, in that the rotary disc between the connection rods rotates clockwise and produces an upward movement of the burst control plate (i.e., h increases). The overall configuration of the burst control plate is illustrated in Fig. 2. By applying the feedback control to adjust the trailing-edge height of the burst control plate, the effectiveness of the plate can be altered. When the burst control plate is not actuated (i.e., its initial position $h = 0$ mm) the authors in the current Note are well aware of the small gaps (i.e., surface discontinuity) located fore and aft of the burst control plate on the airfoil surface.

With the NACA 631-012 airfoil mounted horizontally in the test-section, the aerodynamic forces acting on the airfoil were determined by a three-component external load cell located at 40% of the chord of the airfoil. The load cell has a resolution of $1/16,384$ and the hysteresis is less than 0.5%. The maximum measure limit of the load cell for both the lift and drag components is 60 N. The mean aerodynamic forces were measured with a moderate sampling rate of 512 Hz and no electrical filter was used in the data acquisition system. The load cell was precalibrated in the factory, and the accuracy of the measurement of lift and drag forces acting on the airfoil section are approximately $\pm 0.01\%$. Aerodynamic forces were normalized by the freestream dynamic pressure and airfoil area. Wind-tunnel wall corrections were made based on [10]. The initial tests were conducted on the clean airfoil (i.e., without the installation of the burst control plate) and the results were compared to the airfoil with the plate installation (i.e., the airfoil without the actuation of burst control plate), the airfoil with full actuation (i.e., $h = 1$ mm), and the airfoil with burst control plate autonomous actuation (i.e., the height of the burst control plate is adjusted by the feedback control). Additional tests were conducted to establish the repeatability of the measurements. Note that the angle of attack α of the airfoil section is set by a rotary table, and the uncertainty on the angle of attack is approximately 0.1°.

III. Results and Discussion

A. Feedback Control

Figure 3 shows the block diagram for the smart structure sensor actuator system and its connection to the experimental system. The pressure data are fed by A/D conversion into the PC, in that the data are processed and definitive decisions are made by the PC for the autonomous burst control plate actuation. Through the autonomous actuation (i.e., the plate penetrates into the mainstream) the flow system is altered, and again the pressure sensor records the changes in pressure amplitude and a new cycle of data process begins. To find the rule for the feedback control, the static pressure at $x/c = 0.015$ was investigated at α between 0 and 20° when the actuators were off.

According to the description of the short bubble in [11,12], the existence of the short bubble at the front portion of the airfoil (before the short-bubble burst, typically at $9^\circ \geq \alpha \leq 10^\circ$) causes decreasing pressure, especially within the region of the flow separation and the reattachment. In Fig. 4 when $\alpha < 6^\circ$ the static pressure shows steady increase with the actuator off (i.e., $h = 0$ mm). On the other hand, the authors in the current Note are well aware that the plate penetration into the mainstream at $\alpha < 6^\circ$ causes the reduction of lift (i.e., the plate penetration reduces the suction pressure on the upper side of the airfoil). From the aforementioned reasons, the actuators are programmed to shut off by setting the lower threshold value. As shown in Fig. 4, the slope of the pressure amplitude at $x/c = 0.015$ declines with increasing angle of attack (for $6^\circ \geq \alpha \leq 10^\circ$). This is because the location of the short bubble is moved forward and toward the leading edge of the airfoil. It was conjectured that the plate penetration into the mainstream at $\alpha > 6^\circ$ increases the suction pressure (i.e., lift increases) on the upper surface of the airfoil; thus, the plate is programmed to turn on. As demonstrated in the preliminary study, the suction pressure due to the increasing plate penetration into the flow is significantly higher than the case when the plate is level to the surface at the same angle of attack. On the other hand, each step movement of the plate is triggered by the measured pressure reading that falls within the threshold values, as shown in Fig. 4. Note that this process contains significant hysteresis, a long bubble will result and the control loop is to further increase the plate penetration in the flowfield, and as a consequence thereof, the separated shear layer is forced to reattach on the surface near the leading edge of the airfoil. The sudden decrease in the maximum pressure amplitude (at $\alpha > 10.2^\circ$) of the pressure sensor indicates the short-bubble-burst phenomena at the front portion of the airfoil.

The feedback control system is illustrated by the flowchart shown in Fig. 5. First, the system at $\alpha = 0^\circ$ initializes the height of the burst control plate at $h = 0$ mm (i.e., the actuators are not deployed), and the static pressure level at $x/c = 0.015$ is measured by the pressure sensor. Note that there is a time delay due to the long tubing for the low-pressure measurement. To minimize the potential effect (due to pressure lag) on the actuation of the controller, the time constant of the closed-loop system is set at 100 μs. The system collects a window of data and it stores each window of data as an array in a first-in/first-out stack. Subsequently it calculates the pressure level. The data are then compared with the predetermined upper and lower threshold values (as shown in Fig. 4); if the pressure level is within

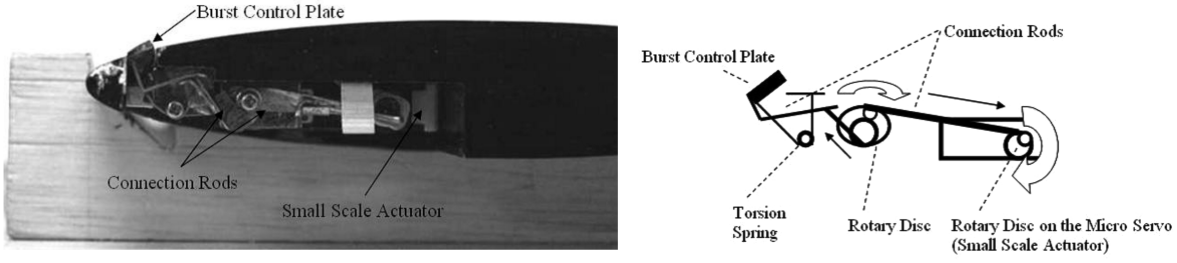

Fig. 2 Front portion of the airfoil section (left) and sketch of the burst control plate actuation (right).

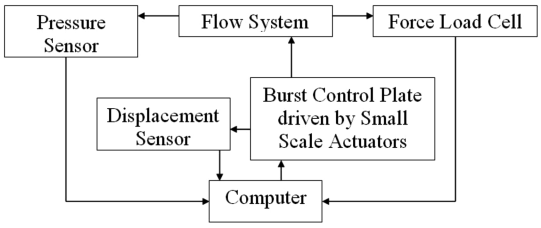

Fig. 3 Diagram of the smart structure sensor actuator system and the experimental system.

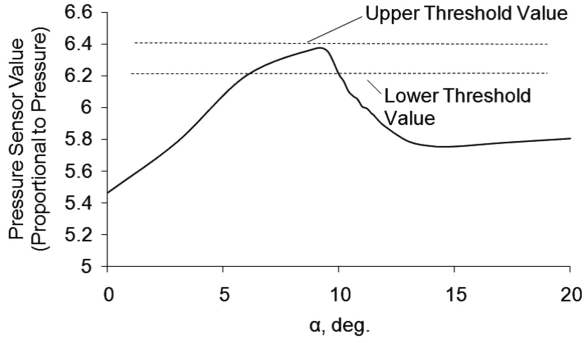

Fig. 4 Representative plot showing pressure sensor value at $x/c = 0.015$ ($U_\infty = 10$ m/s).

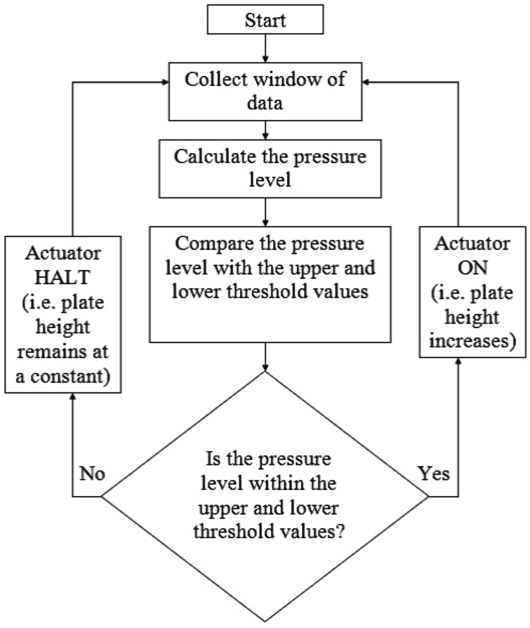

Fig. 5 Flowchart of the pressure-amplitude sense and feedback control method.

the predetermined range of threshold values, the actuator state is set to on, or else the actuator is called to a halt. Note that the lower threshold value and the upper threshold value are 6.22 and 6.40, respectively, at $U_\infty = 10$ m/s. The durations of data acquisition and actuator excitation can be independently adjusted and the angular displacement of the actuators is increased in small steps. The closed-loop cycle repeats itself until the criterion stated in Fig. 5 is not satisfied, then the height of the burst control plate is said to be an optimum. The authors in the current Note must take extra caution for the situation when the burst control plate is beyond its capability for flow reattachment and the movement of the actuators must be called to a halt. This is done by limiting the maximum angular movement of the actuators to approximately 50°, which is equivalent to the height of the burst control plate of about 1 mm.

B. Effectiveness of the Autonomous Actuation on Aerodynamic Forces

A demonstration of the effectiveness of the autonomous actuation system on the aerodynamic forces is presented in Fig. 6. This figure shows the lift coefficient versus the angle of attack α for some cases: the case of clean airfoil (i.e., without the burst control plate installation), the case of airfoil with the actuator being turned off (i.e., $h = 0$ mm), the case of airfoil with the burst control plate at full actuation (i.e., $h = 1$ mm approximately), and the case of airfoil with autonomous actuation (i.e., the height of the burst control plate is adjusted by using the feedback control).

When the angle of attack is set beyond 9°, the pressure amplitude falls within the predetermined threshold values. The control loop triggers the actuators to turn on and the height of the burst control plate increases only when necessary. The maximum lift coefficient of the airfoil at $\alpha = 11.4°$ with autonomous actuation is 3.6% higher than the value of the clean-airfoil case. This result shows that the autonomous actuation system is able to increase the suction pressure at the front portion of the airfoil while maintaining the drag as minimal, as shown in Fig. 7. This is extremely important to avoid the burst control plate moving above or below any height other than its optimum. On the other hand, the autonomous actuation is able to call a halt when the suction pressure is increased above the predetermined upper threshold value.

Figure 7 shows the drag coefficient versus the angle of attack α for the same cases as in Fig. 6. When α lies between 9 and 11.2°, the drag of the case of the airfoil with the actuator being turned off (i.e., $h = 0$ mm) is approximately 16% less than the clean-airfoil case; this is because the drag mainly depends on the location of turbulent boundary-layer separation at the rear portion of the airfoil. When the short bubble is located at the front portion of the airfoil and the burst control plate is not actuated (i.e., $h = 0$ mm), it is suspected that the momentum transfer between the freestream and the flow near the

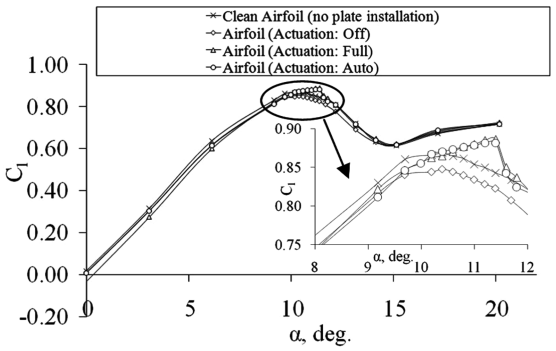

Fig. 6 Lift coefficient versus angle of attack for different cases at $U_\infty = 10$ m/s.

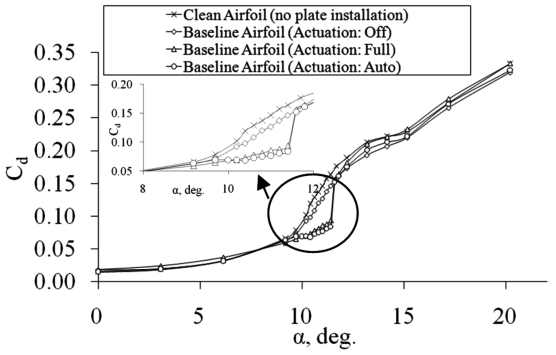

Fig. 7 Drag coefficient versus angle of attack for different cases at $U_\infty = 10$ m/s.

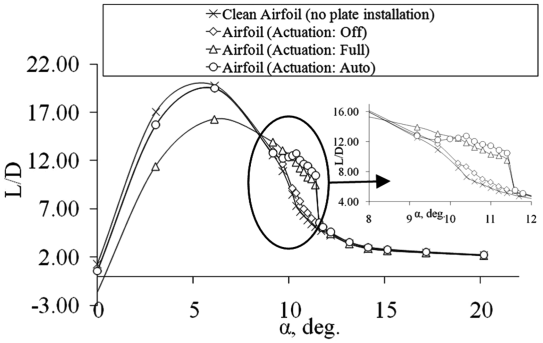

Fig. 8 Lift-to-drag ratio versus angle of attack for different cases at $U_\infty = 10$ m/s.

airfoil surface is enhanced with the presence of the small gaps located fore and aft of the burst control plate. The flow near the surface is more energized and that delays the turbulent boundary-layer separation. For the case of the airfoil with the autonomous actuation, the actuation is triggered (i.e., the plate height increases) when the pressure value lies within the predetermined pressure range. It is noted that the drag of the airfoil with autonomous actuation is approximately 6% less compared with the values of the airfoil with full actuation (i.e., $h = 1$ mm) when α is set above the stall angle of the clean airfoil (i.e., $\alpha = 10.2°$). Herein, the autonomous actuation system demonstrates that it is able to maintain the short bubble from bursting. Note that when α is set at 9 and 10°, the drag of the airfoil with autonomous actuation is approximately 7% higher than the value of the airfoil with full actuation. It is conjectured that the plate penetration in the flowfield adjusted by the autonomous system is insufficient to enhance the flow interactions in the separated shear layer; thus, the delay of turbulent flow separation is limited.

Figure 8 shows the lift-to-drag L/D ratio versus angle of attack α for the same cases as in Fig. 6. Figure 8 illustrates the advantage of the application of the autonomous actuation system and it is more advanced compared with the case of the airfoil with full actuation (i.e., $h = 1$ mm; conventional configuration, as shown in [7]), except when α is between 9 and 10.2°. On the other hand, the increase of drag for the case of autonomous actuation (due to the formation of turbulent boundary layer) when α is between 0 and 6° is avoided and the L/D ratio is maintained approximately the same as with the clean-airfoil case.

When α is between 9 and 10.2°, a trough of L/D ratio exists for case of the airfoil with autonomous actuation. When the suction pressure reduces, the pressure-amplitude sense and feedback control method is capable of detecting and reducing the suction pressure loss by increasing the plate penetration in the flowfield. Once the pressure level lies outside the predetermined pressure range (i.e., the upper and lower threshold values), the actuators are called to a halt (i.e., the height of the burst control plate becomes constant) and the controller becomes less sensitive to other changes in the flowfield: for example, the turbulent intensity of the flow at reattachment. More important, the case of the airfoil with autonomous actuation is the most effective to attain the high L/D (i.e., stall is avoided until α is about 11.2°) and that at the same time L/D is the highest when $10.2° < \alpha < 11.2°$.

IV. Conclusions

The short-bubble burst control using the burst control plate that was incorporated in the smart structure sensor actuator system (in short, autonomous actuation system) was investigated on a NACA 631-012 airfoil section at a chord Reynolds number of 1.3×10^5. A method was developed (namely, the pressure-amplitude sense and feedback control method) for detecting the change in pressure level due to the existence of the short bubble at the front portion of the airfoil and for determining the optimum plate height at different angles of attack. The experiments were intended to validate 1) the feedback rule in the control loop and 2) the effectiveness of the burst control plate with autonomous actuation. The aerodynamic forces acting on the airfoil were investigated by means of total force measurements. The experimental results have shown the following: With the pressure amplitude as the precursors (measured at $x/c = 0.015$), the autonomous actuation system is able to detect the reduction of pressure amplitude due to the existence of the short bubble and to increase the plate height to the optimum. When the optimum plate height is reached, sufficient energy is drawn from the mainstream and that flow reattachment exists. The maximum lift coefficient of the airfoil with autonomous actuation system is increased as compared to the value of the clean airfoil (i.e., no plate installation). Also, the autonomous actuation system is able to avoid the excessive plate height increment, in that the drag of the airfoil with autonomous actuation is effectively minimized. The overall results have proven that the capability of the feedback control approach offers an improvement over the conventional plate configuration, in which the plate height is fixed for all angles of attack. Since the present system is only capable of controlling the flow for airfoil during pitch-up, further research and tests are required to develop some of the concepts to address the issues associated with system integration for airfoil during pitch-down.

Acknowledgments

The research was supported by Japan Society for the Promotion of Science (JSPS). A special thanks to Yasuto Sunada for his beneficial help in all experimental work.

References

[1] Tani, I., *Low-Speed Flows Involving Bubble Separation*, Progress in Aeronautical Sciences, Pergamon, New York, Vol. 5, 1964, pp. 70–103.

[2] Almutairi, P., Jones, L., and Sandham, N., "Intermittent Bursting of a Laminar Separation Bubble on an Airfoil," *AIAA Journal*, Vol. 48, No. 2, 2010, pp. 414–426. doi:10.2514/1.44298

[3] Seifert, A., Darabi, A., and Wygnanski, I., "Delay of Airfoil Stall by Periodic Excitation," *Journal of Aircraft*, Vol. 33, No. 4, 1996, pp. 691–698. doi:10.2514/3.47003

[4] Patel, M., Sowle, Z., Corke, T., and He, C., "Autonomous Sensing and Control of Wing Stall Using a Smart Plasma Slat," *Journal of Aircraft*, Vol. 44, No. 2, 2007, pp. 516–527. doi:10.2514/1.24057

[5] Amir, M., and Kontis, K., "Application of Piezoelectric Actuators at Subsonic Speeds," *Journal of Aircraft*, Vol. 45, No. 4, 2008, pp. 1419–1430. doi:10.2514/1.35630

[6] Rinoie, K., Okuno, M., and Sunada, Y., "Airfoil Stall Suppression by Use of a Bubble Burst Control Plate," *AIAA Journal*, Vol. 47, No. 2, 2009, pp. 322–330. doi:10.2514/1.37352

[7] Wong, C. W., and Rinoie, K., "Bubble Burst Control for Stall Suppression on a NACA 631-012 Airfoil," *Journal of Aircraft*, Vol. 46, No. 4, 2009, pp. 1465–1467. doi:10.2514/1.43924

[8] Segawa, T., Yoshida, H., Nishizawa, A., Murakami, K., and Mizunuma, H., "Sensors and Actuators for Smart Control of Separation," *Theoretical and Applied Mechanics*, Vol. 52, National Comm. for Theoretical and Applied Mechanics, Tokyo, 2003, pp. 117–125.

[9] Nishizawa, A., Takagi, S., Abe, H., Segawa, T., and Yoshida, H., "Smart Control of Separation Around a Wing—Control System," *Proceedings of the Sixth Symposium Smart Control of Turbulence*, Tokyo, March 2005, pp. 9–14.

[10] Allen, H. J., and Vincenti, W. G., "Wall Interference in a Two-Dimensional-Flow Wind Tunnel, with Consideration of Compressibility," NACA Rept. 782, 1944.

[11] Rinoie, K., and Takemura, N., "Oscillating Behaviour of Laminar Separation Bubble Formed on an Aerofoil Near Stall," *The Aeronautical Journal*, Vol. 108, No. 1081, 2004, pp. 153–163.

[12] Rinoie, K., Ichikawa, K., and Sunada, Y., "Behavior of Laminar Separation Bubble Formed on NACA 631-012," *Journal of the Japan Society for Aeronautical and Space Sciences*, Vol. 51, No. 597, 2003, pp. 582–584. doi:10.2322/jjsass.51.582 (in Japanese).